Science Bulletin xxx (2018) xxx–xxx

Contents lists available at ScienceDirect

Science Bulletin

journal homepage: www.elsevier.com/locate/scib

Article

Evidence for a Dirac nodal-line semimetal in $SrAs_3$

Shichao Li [a], Zhaopeng Guo [a], Dongzhi Fu [a], Xing-Chen Pan [a], Jinghui Wang [a], Kejing Ran [a], Song Bao [a], Zhen Ma [a], Zhengwei Cai [a], Rui Wang [b], Rui Yu [c], Jian Sun [a,d], Fengqi Song [a,d,*], Jinsheng Wen [a,d,*]

[a] National Laboratory of Solid State Microstructures and Department of Physics, Nanjing University, Nanjing 210093, China
[b] Department of Physics and Astronomy, Shanghai Jiao Tong University, Shanghai 200240, China
[c] School of Physics and Technology, Wuhan University, Wuhan 430072, China
[d] Collaborative Innovation Center of Advanced Microstructures, Nanjing University, Nanjing 210093, China

ARTICLE INFO

Article history:
Received 9 January 2018
Received in revised form 15 March 2018
Accepted 17 April 2018
Available online xxxx

Keywords:
Dirac nodal-line semimetal
Magnetoresistance
Berry phase
Quantum oscillations
DFT calculations
Chiral anomaly

ABSTRACT

Dirac nodal-line semimetals with the linear bands crossing along a line or loop, represent a new topological state of matter. Here, by carrying out magnetotransport measurements and performing first-principle calculations, we demonstrate that such a state has been realized in high-quality single crystals of $SrAs_3$. We obtain the nontrivial π Berry phase by analysing the Shubnikov-de Haas quantum oscillations. We also observe a robust negative longitudinal magnetoresistance induced by the chiral anomaly. Accompanying first-principles calculations identifies that a single hole pocket enclosing the loop nodes is responsible for these observations.

1. Introduction

Recently, a new type of topological materials, including three-dimensional (3D) Dirac, Weyl, and nodal-line semimetals, have attracted huge interests [1,2]. The Dirac semimetals are analogues to graphene in 3D, with the inverted linear bands crossing at the Dirac nodes near the Fermi level [3]. By breaking either the spatial-inversion (*P*) or time-reversal (*T*) symmetry both present in Dirac semimetals, a fourfold degenerated Dirac node splits into two Weyl nodes with opposite chirality, and these materials are termed Weyl semimetals [4–6]. The low-energy physics of Dirac and Weyl semimetals are described by a Dirac and Weyl equation, respectively [1]. Both Dirac [7–9] and Weyl semimetals [5,10–12] have been established, and shown to exhibit a number of intriguing transport properties, such as the large longitudinal magnetoresistance (MR) and high mobility [9,13–15], nontrivial π Berry phase [16–19], and chiral-anomaly-induced negative longitudinal MR [18,20–25]. Topological nodal-line semimetals, where the linear bands cross each other along a line or loop, instead of at discrete points as in Dirac and Weyl semimetals [26–29], have also been proposed in various systems, including ZrSi*X* (*X* = S, Se, Te) (Refs. [30–32]), Cu_3XN (*X* = Pd, Zn) (Ref. [33]), $XTaSe_2$ (*X* = Pb, Tl) (Ref. [34]), $PtSn_4$ (Ref. [35]), Ca*TX* (*T* = Cd, Ag; *X* = P, Ge, As) (Ref. [36]), Ca_3P_2 (Ref. [37]), and CaP_3 family (Refs. [38,39]). However, many of these proposals, such as the topological nodal-line state in the CaP_3 family, are calling for experimental verification.

The crystal structure of the CaP_3 family contains puckered polyanionic layers stacking along *b* axis, as illustrated in Fig. 1a (Ref. [40]). The material of interest in this work, $SrAs_3$, crystallizes into the monoclinic structure with the C2/m space group [40]. $SrAs_3$ was previously known as a narrow-gap semimetal [40], but a very recent theory work suggested that it was a Dirac nodal-line semimetal protected by *PT* and mirror symmetries, if the spin–orbit coupling (SOC) effect was neglected [38]. Besides, several other members in the CaP_3 family, such as CaP_3, $CaAs_3$, SrP_3, and $BaAs_3$ were also predicted to be such topological semimetals [38,39]. It is highly desirable to realize the predicted topological state in these materials experimentally.

Here, by measuring the magnetoresistance on high-quality single crystals of $SrAs_3$, we observe the nontrivial π Berry phase by analysing the Shubnikov-de Haas (SdH) quantum oscillation data, and the robust negative MR induced by the chiral anomaly. First-principles calculations show that a single hole pocket enclosing the loop nodes is responsible for these exotic properties. These results unequivocally demonstrate that $SrAs_3$ is a Dirac nodal-line semimetal as proposed in Ref. [38].

* Corresponding authors.
E-mail addresses: songfengqi@nju.edu.cn (F. Song), jwen@nju.edu.cn (J. Wen).

https://doi.org/10.1016/j.scib.2018.04.011
2095-9273/

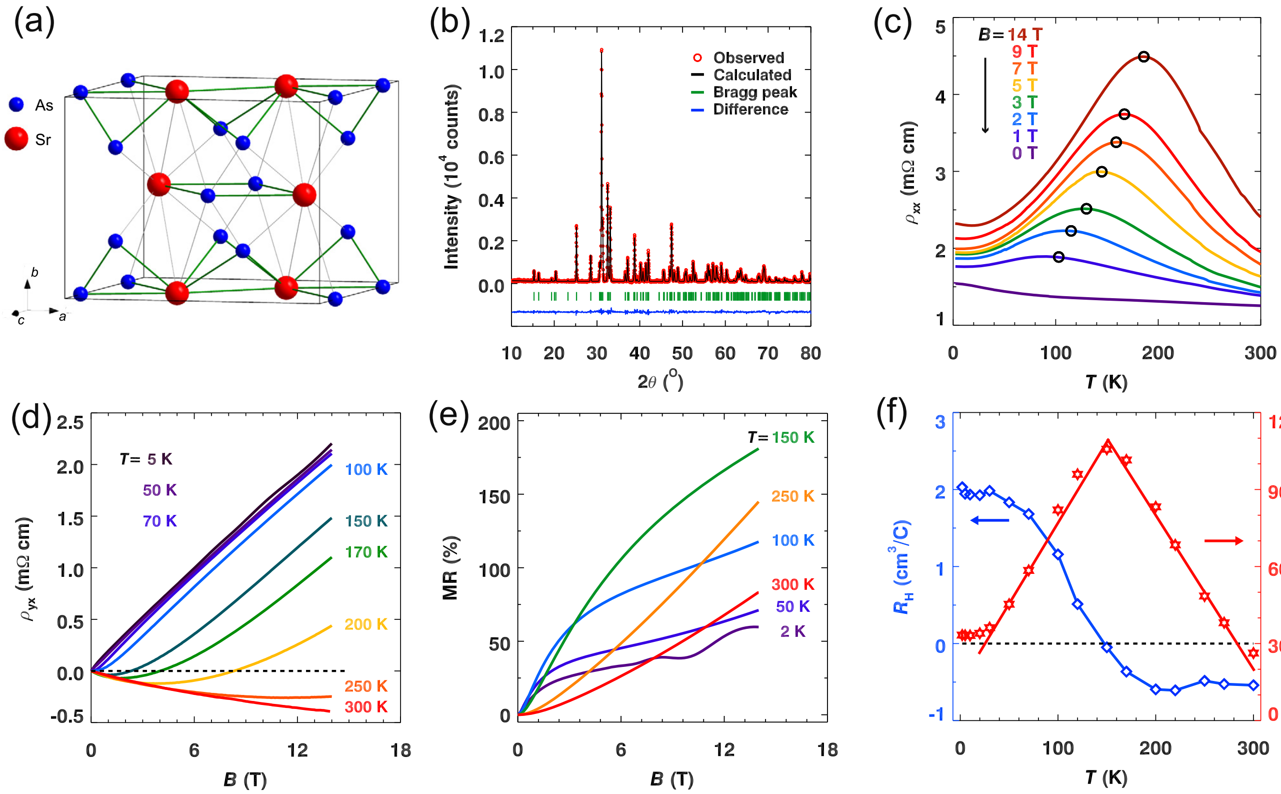

Fig. 1. (Color online) Crystal structure and longitudinal magnetoresistance. (a) Schematic for the crystal structure of $SrAs_3$ (monoclinic, space group C2/m, No. 12). (b) X-ray diffraction patterns measured at room temperature and the refinement results. (c) Temperature dependence of the resistivity (ρ_{xx}) under different magnetic fields. Circles indicate the positions of the turning point at T^*. (d) and (e) Magnetic-field dependence of the Hall resistivity ρ_{yx} and magnetoresistance (MR), respectively. (f) Left, Hall coefficient $R_H(T)$ extracted at $B = 1$ T; Right, MR(T) extracted at $B = 6$ T.

2. Methods

2.1. Sample growth and electrical transport

Single crystals of $SrAs_3$ were grown by melting stoichiometric amounts of Sr and As at 850 °C. After 24 h, the melt was cooled to 750 °C at a rate of 4 °C/h. Then the furnace was shut down and cooled to room temperature. Shiny crystals with size up to $5 \times 3 \times 1$ mm^3 could be obtained so. The crystals have *a-c* plane as the cleavage plane, determined using a Laue X-ray diffractometer, consistent with the stacking arrangement in this material. The composition and structure of the single crystals were measured using a scanning electron microscope equipped with an energy-dispersive X-ray spectrometer (EDS), and a powder X-ray diffractometer, respectively. Refinements of the X-ray diffraction (XRD) data were performed with the FullProf. program. Magnetotransport measurements were performed in a Physical Property Measurement System with a standard six-contact method, which enabled the measuring of the electrical and Hall resistivity simultaneously. The contacts were made on the *a-c* plane of the bar-shape sample.

2.2. DFT calculations

First-principles calculations were performed by using the projected augmented wave method implemented in the Vienna ab initio simulation package [41] based on the generalized gradient approximation in the Perdew-Burke-Ernzerhof functional theory [42]. The energy cutoff of 310 eV was set for the plane-wave basis and a *k*-point mesh of $7 \times 7 \times 7$ was used.

3. Results

3.1. Sample characterization

We first check the composition of the $SrAs_3$ single crystals and confirm that the crystals are stoichiometric with the molar ratio of Sr:As = 1:3. In Fig. 1b, we show the XRD data for $SrAs_3$ powders obtained by grinding the single crystals. It clearly demonstrates that the sample contains a single phase. The XRD pattern can be well indexed with the monoclinic structure (space group C2/m, No. 12), as illustrated in Fig. 1a. From the refinements, we obtain the lattice constants $a = 9.60(8)$ Å, $b = 7.65(8)$ Å, and $c = 5.86(9)$ Å, and $\alpha = \gamma = 90°$ and $\beta = 112.87(0)°$. These results are consistent with the existing literature [40].

3.2. Longitudinal magnetoresistance and Hall resistivity

In Fig. 1c, we plot the temperature dependence of the resistivity (ρ_{xx}) under different magnetic fields for $SrAs_3$ with field B applied perpendicular to the electrical current I. The current flows in the *a-c* plane, not along any particular axis. Under zero field, the temperature dependence of ρ_{xx} is semiconductor-like, but the value of the resistivity is low. These results agree with previous reports on this material [40,43]. Interestingly, when we apply a field, the material undergoes a transition from semiconductor at high temperatures to metal at low temperatures, at a temperature we label as T^*. As can be seen from Fig. 1c, T^* increases monotonically with the field. We believe that this transition is due to the change of the carrier type. In Fig. 1d and 1f, a sign change of the Hall resistivity ρ_{yx} and Hall coefficient R_H from positive (hole) to negative (electron) at T^* upon heating can be clearly observed.